doi:10.1016/j.jmb.2009.08.044 J. Mol. Biol. (2009) 393, 753–764

JMB

Available online at www.sciencedirect.com

ScienceDirect

ELSEVIER

Metal Ion Dependence of Cooperative Collapse Transitions in RNA

Sarvin Moghaddam[1], Gokhan Caliskan[2], Seema Chauhan[3], Changbong Hyeon[4], R. M. Briber[1]*, D. Thirumalai[5]* and Sarah A. Woodson[2]*

[1]*Department of Materials Science and Engineering, University of Maryland, College Park, MD 20472, USA*

[2]*T. C. Jenkins Department of Biophysics, Johns Hopkins University, 3400 N. Charles Street, Baltimore, MD 21218-2685, USA*

[3]*Department of Chemistry, Johns Hopkins University, 3400 N. Charles St., Baltimore, MD 21218-2685, USA*

[4]*Department of Chemistry, Chung-Ang University, Seoul 156-756, Republic of Korea*

[5]*Biophysics Program, Institute for Physical Sciences and Technology, University of Maryland, College Park, MD 20472, USA*

Received 9 July 2009; received in revised form 18 August 2009; accepted 18 August 2009
Available online 25 August 2009

Edited by A. Pyle

Positively charged counterions drive RNA molecules into compact configurations that lead to their biologically active structures. To understand how the valence and size of the cations influences the collapse transition in RNA, small-angle X-ray scattering was used to follow the decrease in the radius of gyration (R_g) of the *Azoarcus* and *Tetrahymena* ribozymes in different cations. Small, multivalent cations induced the collapse of both ribozymes more efficiently than did monovalent ions. Thus, the cooperativity of the collapse transition depends on the counterion charge density. Singular value decomposition of the scattering curves showed that folding of the smaller and more thermostable *Azoarcus* ribozyme is well described by two components, whereas collapse of the larger *Tetrahymena* ribozyme involves at least one intermediate. The ion-dependent persistence length, extracted from the distance distribution of the scattering vectors, shows that the *Azoarcus* ribozyme is less flexible at the midpoint of transition in low-charge-density ions than in high-charge-density ions. We conclude that the formation of sequence-specific tertiary interactions in the *Azoarcus* ribozyme overlaps with neutralization of the phosphate charge, while tertiary folding of the *Tetrahymena* ribozyme requires additional counterions. Thus, the stability of the RNA structure determines its sensitivity to the valence and size of the counterions.

Keywords: RNA folding; SAXS; counterion; ribozyme; singular value decomposition

Introduction

Like proteins, RNA molecules adopt well-defined three-dimensional tertiary structures that are essential for their biological activity. The native tertiary structure is specified by a large number of favorable interactions, such as base stacking and hydrogen bonds, but opposed by the loss of chain entropy and by electrostatic repulsion of the phosphates.[1–3] Consequently, the stability of the folded RNA depends greatly on its preferential interaction with counterions compared to that of the unfolded state.[4]

*Corresponding authors. E-mail addresses: rbriber@umd.edu; thirum@umd.edu; swoodson@jhu.edu.

Present addresses: S. Moghaddam, Center for Advanced Research in Biotechnology, University of Maryland Biotechnology, 9600 Gudelsky Drive, Rockville, MD 20850, USA; G. Caliskan, Teknoloji Yatirimlari ve Danismanlik Sanayi Ve Ticaret A.S., Istanbul, Turkey; S. Chauhan, Xbiotech USA Inc., Austin, TX 78749, USA.

Abbreviations used: SAXS, small-angle X-ray scattering; SVD, singular value decomposition; spd^{3+}, $spermidine^{3+}$; WLC, worm-like chain.

Because RNA is a densely charged polyanion, cations condense around the RNA, reducing the electrostatic repulsion between the phosphate groups and permitting attractive interactions to drive collapse of the RNA chain. After counterion condensation, there is a substantial reduction in the RNA's radius of gyration, R_g, that coincides with a shortening of the persistence length[5] and the initial formation of tertiary structure.[6–10]

The folding of RNAs in the presence of different types of counterions has been studied by both experiment and simulation.[11–14] Small and highly charged cations drive nucleic acid condensation more effectively than do monovalent ions or ions with a large excluded volume.[15–17] First, multivalent ions condense more strongly around the RNA and neutralize a greater fraction of the RNA's negative charge.[18] Second, small ions pack more efficiently around the RNA than large ions.[19–21] In accord with these principles, the folding free energy of the *Tetrahymena* group I ribozyme decreases linearly with the charge density of the counterions, with the folded RNA being most stable in small divalent ions such as Mg^{2+}.[22]

Coarse-grained molecular simulations and experiments in which metal ions are replaced with polyamines showed that this correlation depends primarily on the valence and size of the counterions and not on site-specific interactions between the ions and the RNA.[19–22] These nonspecific "polyelectrolyte effects" minimally include the electrostatic attraction of counterions to the RNA, interactions between condensed counterions, and the displacement of co-ions from the vicinity of the RNA.[23] The irregular structures of certain RNAs also create opportunities for site-specific metal ion binding and the chelation of tightly bound ions (e.g., Refs. 24–28), but the net free energy gained from such interactions is diminished by the large and unfavorable free energy of ion dehydration.[4]

The *Tetrahymena* L-21 ribozyme forms its native structure through metastable intermediates, in which one domain of its tertiary structure (P4–P6) is folded,[29,30] while the other domain (P3–P9) is partially mispaired.[31] When the ribozyme is refolded in the presence of Mg^{2+}, the formation of these folding intermediates correlates with several transitions in which the average R_g becomes smaller.[10,32] By contrast, the smaller thermostable group I ribozyme from the bacterium *Azoarcus* sp. B72 folds via compact intermediates (I_C) that resemble the native state.[33,34] The collapse transition from the unfolded state (U) to I_C, which occurs in 0.3–0.4 mM $MgCl_2$, coincides with sequence-specific assembly of the core helices.[9] A second transition at 2–3 mM $MgCl_2$ from I_C to the native state (N) correlates with the onset of ribozyme activity.[33]

To address the importance of polyelectrolyte effects *versus* sequence-specific interactions of metal ions with the RNA, we compared the equilibrium collapse transitions of the *Azoarcus* and *Tetrahymena* ribozymes in the presence of various metal cations, using small-angle X-ray scattering (SAXS). The effects of counterions on folding of these ribozymes were previously measured using native gel electrophoresis or biochemical assays.[18,20,22,29,35–38] X-ray scattering at small angles is sensitive to structural features in the range of 1–100 nm and is particularly useful for characterizing unfolded and partially folded states of biomolecules that are not readily studied by NMR or X-ray crystallography.[39,40] SAXS has been successfully used to monitor changes in the overall size and shape of several ribozymes and tRNA as the RNA folds.[7,34,41,42]

Using singular value decomposition (SVD) of SAXS spectra, we report that both ribozymes undergo cooperative collapse transitions to native-like conformations in all of the counterions tested, consistent with the ability of many different cations to induce folding of the RNA.[18,29] The cooperativity of this transition depends on the valence and size of the counterion. For both RNAs, collapse correlates with the formation of its tertiary structure, and thus involves specific folding as well as polyelectrolyte effects. However, in the *Azoarcus* ribozyme, collapse overlaps with neutralization of the phosphate charge by the counterions, while in the larger *Tetrahymena* ribozyme, these two steps are distinct, consistent with the presence of metastable folding intermediates.[29–31] We discuss how the sequence-encoded folding pathway and the charge density of the counterions contribute to the cooperativity and specificity of RNA folding.

Results

Change in ribozyme conformation by SAXS

To determine how cations influence the collapse transition (as opposed to tertiary folding), we used SAXS to follow the structure of the *Azoarcus* and *Tetrahymena* ribozymes in cations with different charge or size. Figure 1a and c shows the scattering intensity $I(Q)$ for the *Azoarcus* and *Tetrahymena* ribozymes as the concentration of Mg^{2+} increases from 0.0 to 7 or 5 mM, respectively. The systematic variation in $I(Q)$ in the Q region between 0.008 and 0.11 $Å^{-1}$ correlates with the expected decrease in the average size of the RNA and the transition from a stiff coil with no added Mg^{2+} to a globule in ≥ 5 mM Mg^{2+}. The transition to a globular form was also apparent from Kratky plots of the unfolded and folded RNA, with a pronounced maximum appearing for the folded states of both ribozymes (Fig. S1).

The scattering curves were inverted to obtain the real space distance distribution functions, $P(r)$, as described in Materials and Methods (Fig. 1b and d). As Mg^{2+} is titrated to ≥ 5 mM, the maximum value of D_{max} decreases from 200 to 85 Å for the *Azoarcus* ribozyme, and from 240 to 110 Å for the *Tetrahymena* ribozyme. Values of D_{max} were systematically varied to obtain the best fits to the experimental scattering curves (see Materials and Methods). In low concentrations of Mg^{2+} (< 0.44 mM), the $P(r)$

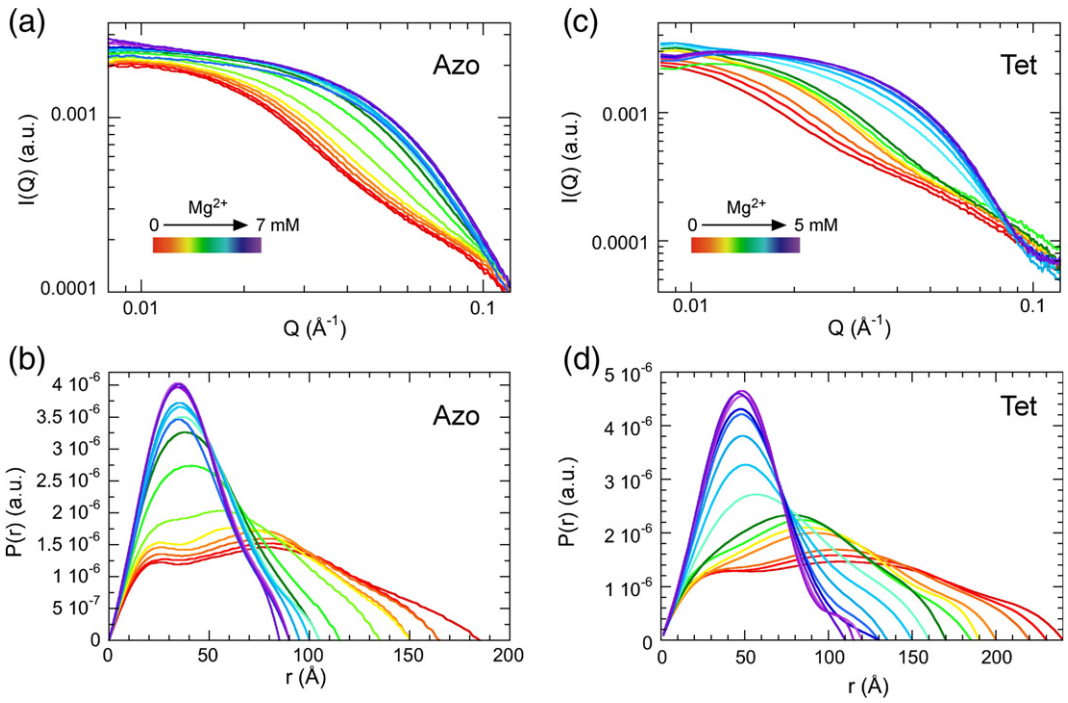

Fig. 1. Small angle X-ray scattering of ribozymes. (a and c) Scattering intensity $I(Q)$ *versus* Q at 32 °C. (b and d) Distance distribution function, $P(r)$, at various Mg^{2+} concentrations (see Materials and Methods). The symbols are the same as in (a) and (c). (a and b) *Azoarcus* ribozyme (Azo; 195 nt) in 20 mM Tris–HCl and 0 (red) to 7 (purple) mM $MgCl_2$. (c and d) *Tetrahymena* ribozyme (Tet; 389 nt) in 20 mM Tris–HCl, plus 0 (red) to 5 (purple) mM $MgCl_2$.

function shows two maxima, consistent with the two lobes of scattering density, which disappear as the Mg^{2+} concentration is increased and the RNAs collapse to a smaller set of compact conformations. The $P(r)$ function was used to calculate R_g at each ion concentration. Similar R_g values were obtained using the Guinier approximation.

Cooperative counterion-dependent collapse of the *Azoarcus* ribozyme

We previously reported a cooperative transition in the *Azoarcus* ribozyme from the unfolded form in 20 mM Tris–HCl with $R_g = 65$ Å to a compact form in ≥ 3 mM Mg^{2+} with $R_g = 31$ Å, as observed by both small-angle neutron scattering and SAXS.[9,34] The experimentally determined R_g of the folded ribozyme is similar to the value of 31.1 Å[9] calculated from the crystal structure of the *Azoarcus* ribozyme.[43] The midpoint of the Mg^{2+}-induced collapse transition revealed by SAXS (0.34 mM) superimposes on biochemical and spectroscopic measures of helix assembly and can be approximated by a two-state folding model.[9,34]

Although the two-state approximation is accurate near the transition midpoint,[9] it neglects changes in the unfolded ensemble as the Mg^{2+} concentration changes and the differences between I_C and N. Differences between I_C and N were revealed as a small plateau in the Mg^{2+} titration at $R_g = 33$ Å just after the main collapse transition, followed by a decrease in R_g to 30 Å between 2 and 7 mM $MgCl_2$ (Fig. 2a). This additional compaction of the ribozyme, which is barely larger than the uncertainty of the SAXS measurements, occurred in the same Mg^{2+} concentration range as the transition from I_C to N defined by the onset of splicing activity.[33,44] We have previously ascribed a gradual change in the scattering function at the beginning of the Mg^{2+} titration to a contraction of the unfolded ensemble.[9]

Assuming that the main collapse transition between U and I_C can be approximated by a two-state model (up to 3 mM $MgCl_2$), the fraction folded RNA at each ion concentration was calculated from R_g^2.[7] The midpoint C_m and cooperativity n of the folding equilibrium[45] was estimated from the Hill equation [Eq. (4); Materials and Methods]. We take n to represent the change in folding free energy with respect to ion concentration. Using these assumptions, we found the cooperativity of the collapse transition with respect to Mg^{2+} concentration was 3.7 ± 0.4 (Table SI).

We next empirically modeled the decrease in R_g (U) by fitting the data at low ion concentrations (below the start of the collapse transition) to a logarithmic function (see Materials and Methods and Fig. S2). When this correction to R_g(U) was extrapolated across the Mg^{2+} titration range, the remaining difference between the unfolded and folded states fit the two-state model extremely well over the entire transition window (up to 3 mM) (Fig. S2). The apparent cooperativity of the collapse transition in Mg^{2+} increased to 6.5 ± 0.9 (Table 1). Although the correction to R_g(U) is based on a small number of data points and should be regarded with

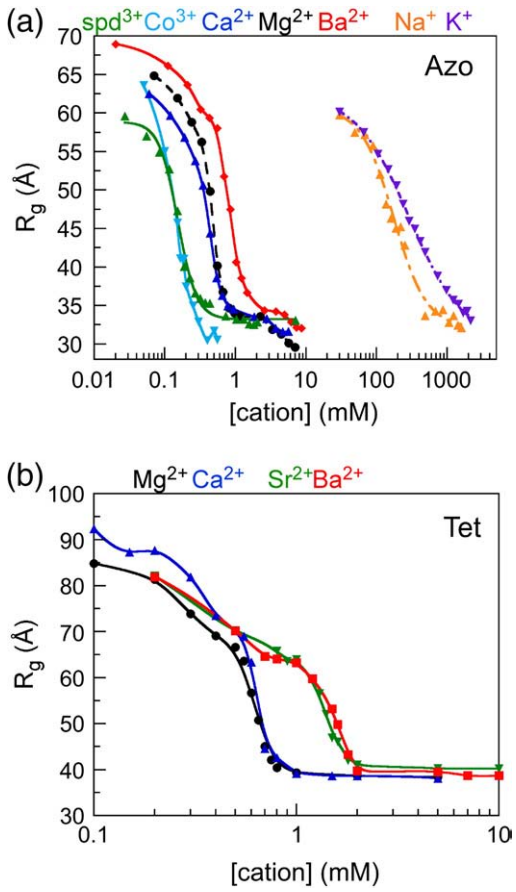

Fig. 2. Counterion induced collapse by SAXS. The radius of gyration (R_g) obtained from $P(r)$ (see Materials and Methods) *versus* cation concentration at 32 °C. Similar results are obtained from the Guinier approximation. (a) *Azoarcus* ribozyme in spd^{3+} (green), Mg^{2+} (black), Ca^{2+} (blue), Ba^{2+} (red), Na^{+} (orange) and K^{+} (purple). $[Co(NH_3)_6]^{3+}$ not shown. Lines represent a smooth curve. See Fig. S2 for fits to ϕ_U *versus* C. (b) *Tetrahymena* ribozyme in Mg^{2+} (black), Ca^{2+} (blue), Sr^{2+} (green) and Ba^{2+} (red). See Fig. S4 for fits to a three-state model.

caution, it did not alter the qualitative differences among the counterions.

Counterion valence and size

To probe the contribution of polyelectrolyte effects, we compared the cooperativity of the collapse transition measured by SAXS in monovalent, divalent, and trivalent cations. As expected from previous hydroxyl radical footprinting experiments,[36] the *Azoarcus* ribozyme was able to fold in all of the ions tested, which were Na^{+}, K^{+}, Mg^{2+}, Ca^{2+}, Ba^{2+}, $[Co(NH_3)_6]^{3+}$, and spermidine^{3+} (spd^{3+}) (Fig. 2a). The R_g values were similar, and thus the static volume of the native RNA does not depend strongly on the valence or ionic radius of the metal ions compared here. However, a comparison of the $P(r)$ functions for ribozyme folded in the different cations revealed small differences in the average structure of the RNA (Fig. 3a). Mg^{2+} and the other divalent ions produced the most compact and well-folded structure, while K^{+} and spd^{3+} produced more asymmetrical $P(r)$ distributions with a slightly larger D_{max} (95–100 Å). The value of D_{max} is an indication of the largest fluctuations in the RNA. The R_g of the folded ribozyme was slightly larger (32–33 Å) in monovalent ions than in Mg^{2+} (30 Å) (Table 1), consistent with the inability of monovalent ions to correctly organize the ribozyme active site.[36]

Table 1. Counterion-dependent collapse of the *Azoarcus* ribozyme at 32 °C

Cation	r (Å)[a]	R_g (N) (Å)[b]	C_m (mM)	n_H
Na^{+}	2.41	32.1	186±15	2.0±0.3
K^{+}	2.70	33.0	356±14	1.3±0.05
Mg^{2+}	2.07	30.0	0.48±0.01	6.5±0.9
Ca^{2+}	2.33	31.6	0.45±0.01	5.5±0.8
Ba^{2+}	2.99	32.2	0.81±0.02	4.2±0.4
$[Co(NH_3)_6]^{3+}$	2.06	30.5	0.13±0.009	3.5±0.9
spd^{3+}	4.5	32.6	0.14±0.004	3.1±0.2

The midpoints (C_m) and Hill constants (n_H) were obtained from fraction unfolded RNA (ϕ_U) *versus* cation concentration fit to Eq. (4) as described in Materials and Methods. Errors listed in the table are from the statistics of the fit. $R_{g,U}$ at each counterion concentration (C) was empirically extrapolated from the data at low C: Mg^{2+}, $R'_{g,U}=52.3-11(\log C)$; Ca^{2+}, $R'_{g,U}=47-13(\log C)$; Ba^{2+}, $R'_{g,U}=59-6.4(\log C)$. Fits to individual data sets are shown in Fig. S2; parameters obtained without correcting $R_{g,U}$ are given in Table SI. Errors listed in the table are from the statistics of the fit.

[a] Length of the M–O bond for hydrated ions and the Co–N bond for cobalt hexammine. For spd^{3+}, r is half the approximate length of the polyamine.

[b] Average R_g in highest cation concentrations tested. The uncertainty in R_g is approximately 1 Å for N and 3–5 Å for U.

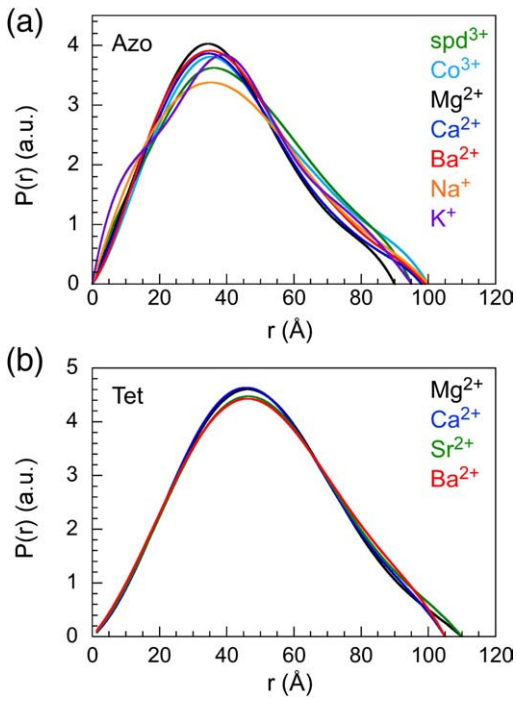

Fig. 3. Structure of the folded RNA in different cations. Comparison of $P(r)$ for the folded RNA in various counterions as indicated in the key. Functions were normalized to the area under the curve. (a) *Azoarcus* ribozyme. (b) *Tetrahymena* ribozyme.

Higher concentrations of Na^+ and K^+ than those of divalent or trivalent ions were needed to stabilize the compact form of the *Azoarcus* ribozyme, consistent with the stronger ability of multivalent cations to stabilize folded RNA structures.[4,18,46] The midpoints for collapse transitions in Mg^{2+}, Ca^{2+} and Ba^{2+} were 0.45 to 0.8 mM (Table 1), while trivalent cations $[Co(NH_3)_6]^{3+}$ and spd^{3+} were effective at 120–140 μM. The midpoints in Na^+ and K^+ were about 190 and 350 mM, respectively (Table 1). In contrast with multivalent ions, the collapse transition in monovalent ions requires more salt than base-pairing of core helices (50 mM), but instead overlaps with tertiary folding probed by hydroxyl radical footprinting (150 mM).[36] The transitions induced by Na^+ and K^+ were also significantly less cooperative (n=1–2) than those in multivalent ions (n=3–6.5; Table 1). Thus, multivalent cations stabilize compact forms of the RNA much more effectively than monovalent cations.

When titrations in counterions with the same valence were compared, we found that small ions stabilized the compact state more efficiently than large ions, as observed in previous folding assays on the *Tetrahymena* and RNase P ribozymes and other RNAs[18,26,29,47] and the biochemical footprinting of the *Azoarcus* ribozyme in divalent and monovalent salts.[36] Folding in Ba^{2+} was less cooperative and had a higher midpoint (0.8 mM) than folding in small ions such as Mg^{2+} and Ca^{2+} (0.5 mM; Table 1). Similar differences were observed between Na^+ and K^+. We also found that although the transition midpoints in the polyamine spd^{3+} and the smaller metal complex $[Co(NH_3)_6]^{3+}$ were nearly the same, the $P(r)$ functions showed that the RNA was much more extended throughout the collapse transition in spd^{3+} (Fig. S3). In general, the stability of the I_C state in the *Azoarcus* ribozyme deduced from the change in R_g was less sensitive to counterion size than the folded form of the *Tetrahymena* ribozyme, as discussed below.

Counterion-dependent collapse of the *Tetrahymena* ribozyme

To further address the effect of counterion size on the collapse transition in RNA, we titrated the *Tetrahymena* ribozyme with the alkaline earth metal ions Mg^{2+}, Ca^{2+}, Sr^{2+} and Ba^{2+}. The R_g at each ion concentration was obtained from the $P(r)$ functions as described above. In all four divalent ions, the *Tetrahymena* ribozyme folded in two well-separated transitions as the cation concentration was raised (Fig. 2b). The R_g of the unfolded ribozyme in 20 mM Tris–HCl was 85–90 Å. In 0.5 mM $MgCl_2$, the R_g reached an intermediate value of ~64 Å. As more ions were added, R_g dropped sharply, reaching the minimum value of 38 Å above 1 mM $MgCl_2$. The scattering data of the folded state (N) agreed well with the $P(r)$ function and R_g=37.4 Å calculated from the three-dimensional model of the full-length ribozyme[48] using the program CRYSOL.[49] The other divalent metal ions produced a similar folded state with R_g=38–40 Å (Fig. 3b). The folded *Tetrahymena* ribozyme was previously reported to have R_g=47 Å[32,42] at 25 °C.

The results on the *Tetrahymena* ribozyme were fit to a three-state model (U ⇔ I ⇔ N), in which the free energies of the I and N states relative to the U state are assumed to decrease with $\ln[Mg^{2+}]$ [Eq. (6); Materials and Methods]. The experimental values of R_g^2 were fit to the three-state model to obtain the populations of the I and the N states and the average R_g of the I state (Table SII and Fig. S4). The midpoints of the U to I and I to N transitions were then calculated from the populations of U and N, respectively (Table 2).

Figure 2b shows that the first transition to more compact structures, which is centered on 0.3 mM, is very similar in all four divalent ions. By contrast, the second transition to the native-like folded state (N) is not only more cooperative, but depends much more strongly on the size of the counterion. In the smallest ions (Mg^{2+} and Ca^{2+}), this transition has a midpoint of 0.63 mM ion, while in the largest ions (Sr^{2+} and Ba^{2+}), it occurs at 1.4 and 1.5 mM ion (Table 2). In addition, the folded state formed less cooperatively with respect to Sr^{2+} and Ba^{2+} concentration than Ca^{2+} and Mg^{2+} concentration.

SVD of collapse transitions

To estimate the number of intermediates in the collapse transitions of the *Azoarcus* and *Tetrahymena* ribozymes, we performed SVD on the scattering intensities at different Mg^{2+} concentration for both ribozymes (see Materials and Methods). The minimum number of basis functions, L, needed to describe the scattering data, was determined by reconstructing the scattering profiles using Eq. (7) (see Materials and Methods). The first three basis functions for the *Azoarcus* and *Tetrahymena* ribozymes weighted by their corresponding singular values are shown in Fig. S5.

As illustrated in Fig. 4a and b, just two basis functions were required to reconstruct the experimental scattering curves for the unfolded and folded *Azoarcus* ribozyme. Only a small improvement in the fit to the unfolded state data was obtained by including a third component. On the other hand, the scattering data for the *Tetrahymena* ribozyme in low Mg^{2+} were only described by three or more basis

Table 2. Counterion-dependent collapse of the *Tetrahymena* ribozyme at 32 °C

Cation	R_g(N) Å[a]	$C_{m,I}$ (mM)	n_I	$C_{m,F}$ (mM)	n_F
Mg^{2+}	38.5	0.28±0.01	3.4±0.4	0.63±0.01	13±2
Ca^{2+}	38.0	0.30±0.01	2.7±0.3	0.64±0.01	17±4
Sr^{2+}	40.2	0.30±0.01	2.5±0.2	1.36±0.02	9±1
Ba^{2+}	38.9	0.31±0.01	2.5±0.2	1.52±0.04	9±1

Apparent midpoints (C_m) and Hill coefficients (n) for the U to I and I to N transitions, respectively, calculated from populations of U and N predicted by the three-state model [Eq. (6)]. See Table SII for fit parameters to Eq. (6) used to calculate the populations of U, I and N as shown in Fig. S4. Errors given in the table are based on the three-state fits.

[a] Average R_g of the folded or native ribozyme.

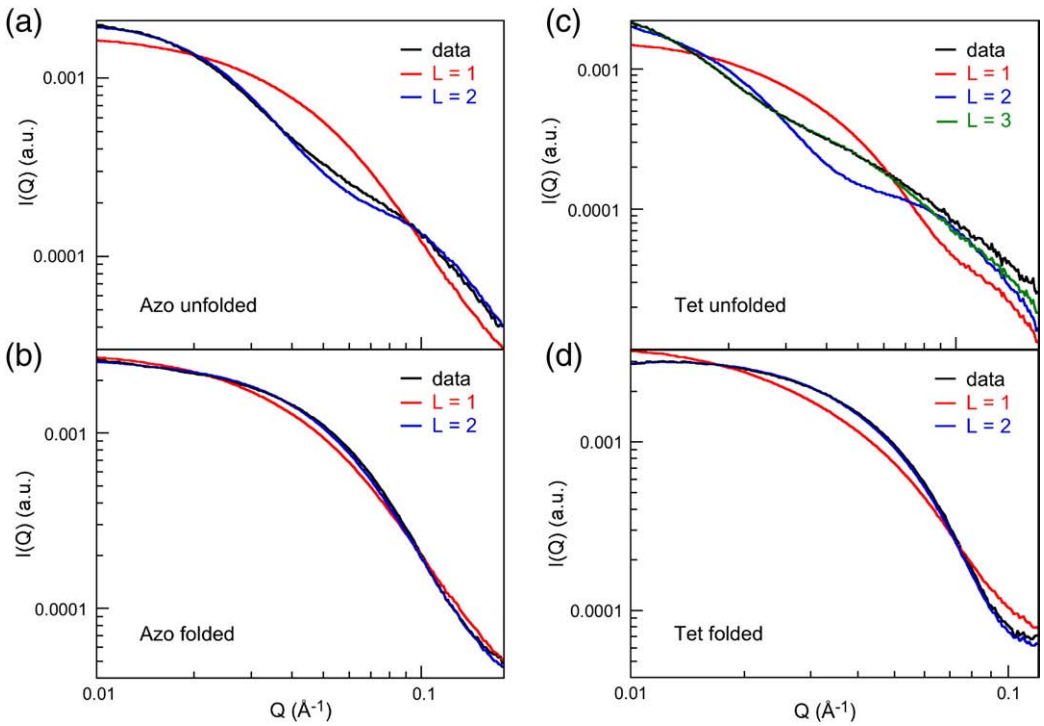

Fig. 4. SVD analysis reveals minimum components of scattering data. Experimental scattering data [($I(Q)$ *versus* Q] (black) are compared with SVD analysis using one to three basis functions; $L=1$ (red), $L=2$ (blue); $L=3$ (green). (a) Unfolded *Azoarcus* ribozyme in 20 mM Tris–HCl. (b) Folded *Azoarcus* ribozyme in 7 mM $MgCl_2$. (c) Unfolded *Tetrahymena* ribozyme in 20 mM Tris–HCl. (d) Folded *Tetrahymena* ribozyme in 5 mM $MgCl_2$.

functions ($L=3$) (Fig. 4c and d). The presence of an additional component is consistent with the presence of a folding intermediate for the *Tetrahymena* ribozyme that is less compact than the folded state. The minimum number of basis functions required to describe the scattering data for each ribozyme over the range of Mg^{2+} concentrations studied was consistent with the values of χ^2, which showed a reasonable quality of fit with the reported number of basis functions.

The weighting factors of the basis functions for the *Azoarcus* and *Tetrahymena* ribozymes for different Mg^{2+} concentrations reflect the folding transition (Fig. 5). The weighting factor for the dominant basis function U_1, which is characteristic of the scattering from a globular shape (Fig. S5), increases sharply through the midpoint of the collapse transition. The weighting factor for the third basis function is close to zero for the *Azoarcus* ribozyme, consistent with a two-state folding transition (continuous green line, Fig. 5). For the *Tetrahymena* ribozyme, the weighting factor of the third component fluctuates around the midpoint of the collapse transition, consistent with the presence of an intermediate (dashed green line, Fig. 5). Therefore, the SVD analysis supports our conclusion that the collapse transition of the *Azoarcus* ribozyme can be approximated by two states, while that of the *Tetrahymena* ribozyme involves at least one equilibrium intermediate, as expected from previous biochemical and time-resolved SAXS experiments on the *Tetrahymena* ribozyme.[29,30,32]

Persistence lengths from *P*(*r*)

Single-molecule experiments on a number of RNAs and analyses of many structures from the Protein Data Bank show that a worm-like chain (WLC) model describes the global shape of RNA

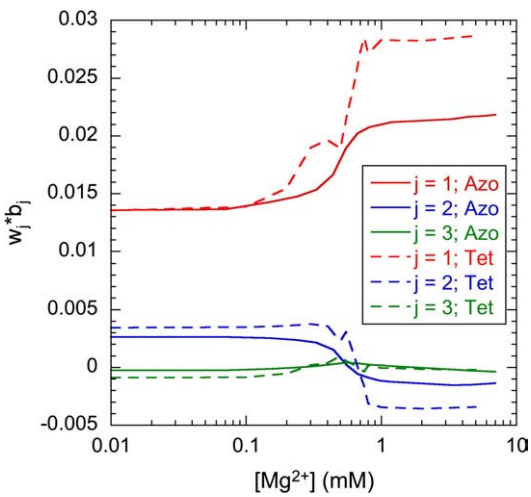

Fig. 5. An intermediate in compaction of the *Tetrahymena* ribozyme. Weighting factors from the SVD analysis (w_jb_j) *versus* Mg^{2+} concentration for the *Azoarcus* ribozyme (continuous lines) and *Tetrahymena* ribozyme (dashed lines). w_1b_1 (red), w_2b_2 (blue), and w_3b_3 (green). The third component (green) contributes to the scattering data at the collapse transition of the *Tetrahymena* ribozyme but not the *Azoarcus* ribozyme.

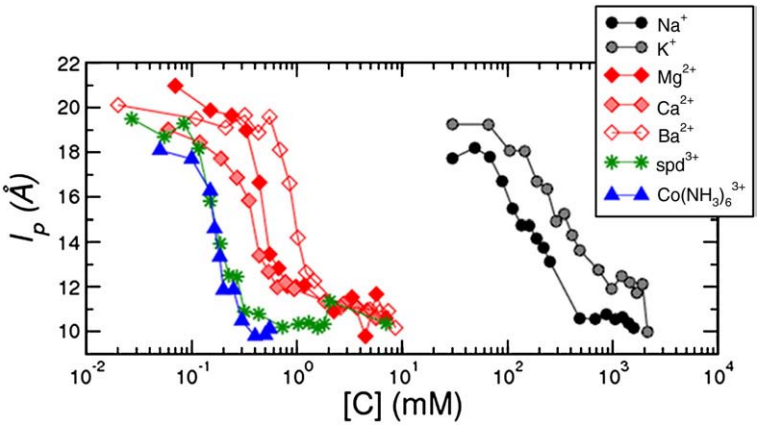

Fig. 6. Ion-dependence of RNA persistence length. The persistence length (l_p) of the *Azoarcus* ribozyme at each ion concentration C was obtained from WLC fits to $P(r)$ [Eq. (10)]. The symbols for the different ions are shown in the key.

molecule.[50,51] We extracted the persistence length, l_p, from the SAXS data by fitting the distance distribution function $P(r)$ for $r > R_g$ to the WLC model in Eq. (10).[5] This model fit the data at large r extremely well, allowing us to obtain l_p for all the counterions.

The persistence lengths of the folded and unfolded RNA are essentially the same in all counterions. Regardless of the counterion, the persistence length decreased from about 20 Å at low counterion concentrations to about 10 Å in the folded state (Fig. 6). The value $l_p \approx 10$ Å in the folded state was also obtained by fitting the force-extension curves for RNA molecules to the WLC model.[50]

At the midpoints of the transitions (Table 1), l_p is 14–17 Å. These values are closer to l_p of the unfolded state, showing that even in the transition region, the RNA chain remains somewhat stiff (larger l_p), and hence the probability of forming tertiary interactions is small. Consequently, the transition to the folded state likely occurs closer to the unfolded structure, particularly in low-charge-density (ζ) ions (spd^{3+} and Ba^{2+}) in which $l_p \sim 17$ Å at C_m.

Discussion

We have used SAXS to compare the collapse transition of the *Azoarcus* and *Tetrahymena* ribozyme in different cations. Although SAXS cannot reveal structural details, such as the conformation of an active site, it provides a physical measurement of the average chain conformation in solution. The equilibrium folding pathways of the *Azoarcus* and *Tetrahymena* ribozymes monitored by SAXS are consistent with previous biochemical and spectroscopic studies of these RNAs.[52,53] By comparing the compaction of these RNAs in different ions, we obtain further insight into the roles of RNA sequence and counterion size and valence in the folding process.

The smaller and more thermostable *Azoarcus* ribozyme goes through a cooperative collapse transition from an expanded state U to a compact intermediate I_C whose dimensions are barely distinguishable from those of the native (N) ribozyme (Fig. 7).[9,34] Mutational studies showed that the collapse transition of this ribozyme coincides with the establishment of tertiary interactions,[9] helping to explain why I_C is nearly as compact as N. Since the SVD analysis demonstrates that only two components are needed to reconstruct the scattering data across the Mg^{2+} titration, other conformational states must be either unpopulated or have scattering functions similar to those of U and N (or U and I_C). Although the *Azoarcus* ribozyme is only biologically active in Mg^{2+}, previous footprinting data showed that other metal cations stabilize a folded conformation (I_F) that contains most of the expected tertiary interactions.[36] This explains why the average structure of the folded ribozyme measured by SAXS is so similar in different ions.

Although the collapse transition for the *Azoarcus* ribozyme can be treated as a two-state folding reaction, this approximation is imperfect over the lowest range of ion concentrations tested (Fig. 7). The extent to which the two state approximation breaks down can be assessed using $\Delta P(r|C) = |[P(r) - (\phi_U P_U(r) + (1-\phi_U)P_F(r))]|$ where $P_U(r)$ and $P_F(r)$ are the distance distribution functions at low and high counterion concentrations, respectively. As an illustration, we calculated $\Delta P(r|C)$ for Mg^{2+} and found that $\Delta P(r|C)$ is not negligible, especially around the transition midpoint (Fig. S6). This suggests that structures other than those in the U or I_C states also determine the cooperativity of the collapse transition. Alternatively, it is likely that there are changes in the unfolded state as the counterion concentration changes, so that the assumption that $P_U(r)$ does not depend on counterion concentration is not strictly valid.

In contrast to the *Azoarcus* ribozyme, the ion titrations and SVD analysis revealed at least two well-separated equilibrium folding transitions for the *Tetrahymena* ribozyme in divalent metal ions, consistent with many experiments showing that this RNA folds through metastable, non-native intermediates.[52,54] The initial transition produces intermediates (I) that are much less compact than the native RNA ($R_g \approx 64$ Å), while the second and more cooperative transition leads to a folded state (N) that has the R_g expected for the native RNA

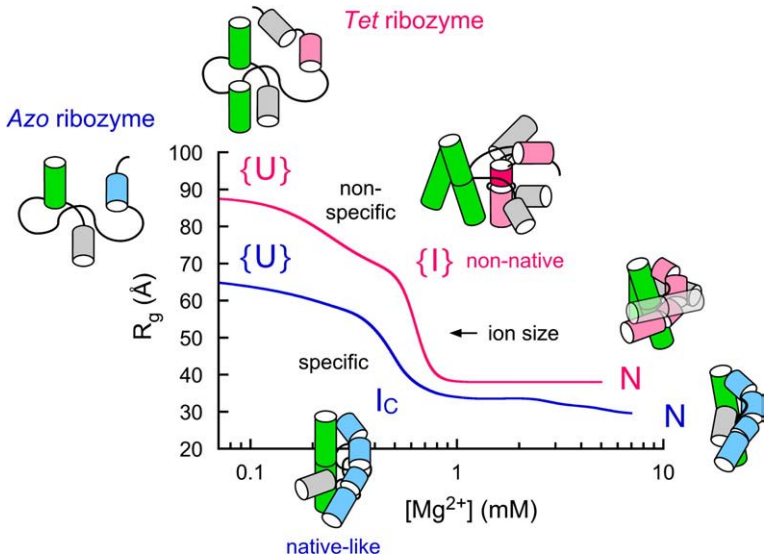

Fig. 7. Mechanism of counterion collapse at equilibrium. For the *Azoarcus* ribozyme (blue), neutralization of the phosphate charge results in cooperative collapse of the unfolded ensemble (U; R_g = 60–70 Å) to native-like intermediates (I_C; R_g = 32–33 Å). This is followed by slightly tighter packing in the native state (N in Mg^{2+} or I_F in other ions; R_g = 30 Å). The unfolded state, which contains some secondary structure, likely changes as the Mg^{2+} concentration is raised. For the less stable *Tetrahymena* ribozyme (red), neutralization of the phosphate charge in the unfolded state (R_g = 80–90 Å) produces intermediates (I; $R_g \approx 64$ Å) that are less structured than the native state (N; R_g = 38 Å). For both RNAs, the transition to N becomes more cooperative when counterion charge density is high.

(38 Å) (Fig. 7). In the SVD analysis, the third component contributes to the scattering intensity near the transition midpoint, as expected for an intermediate (Fig. 5).

It has been proposed that the first transition of the *Tetrahymena* ribozyme corresponds to increased flexibility (and thus contraction) of the unfolded RNA after neutralization of the phosphate charge, while the second transition corresponds to the formation of tertiary structure.[8,10] In previous SAXS studies, a transition to $R_g \sim 45$ Å correlated with the formation of stable tertiary interactions in the independently folding P4–P6 domain, and to a lesser extent, in other peripheral domains of the ribozyme.[38] Time-resolved SAXS experiments at 25 °C uncovered kinetic intermediates with values of R_g between 60 and 45 Å[8,10,32] that correlate with folding intermediates detected by footprinting and other biochemical probes.[30,55,56] In our titrations, the folded state has R_g = 38 Å, which we infer requires proper folding of the ribozyme core. The lower R_g obtained here under equilibrium conditions, compared with earlier SAXS studies, may be due to frequent mispairing of the core and the very long times required to refold the *Tetrahymena* ribozyme at low temperatures.[31,57]

We propose that to a large extent, polyelectrolyte effects drive both RNAs toward more compact structures as the counterions neutralize the negative charge on the phosphates. However, the different stabilities of the intrachain interactions in the two RNAs produce different outcomes (Fig. 7). For the more stable *Azoarcus* ribozyme, the dominant collapse transition occurs with the assembly of core helices and initial tertiary interactions between domains,[9] thus ensuring the formation of native-like intermediates. Hence, specific collapse to I_C occurs in the same window of counterion concentration as the initial charge neutralization of the unfolded ensemble.

In the *Tetrahymena* ribozyme, the catalytic core is less stable and requires more counterions to fold correctly. Thus, charge neutralization initially produces an intermediate ensemble that is less compact ($R_g \sim 64$ Å) than the native state (R_g = 38 Å). In keeping with this idea, the first transition leading to I reaches its midpoint (0.3 mM) when the number of positive charges from the counterions (0.6 mM) is half the number of phosphodiesters in the sample (1.2 mM). The transition to I appears less specific than the transition leading to N in that it is weakly cooperative with respect to ion concentration and insensitive to the size of the counterion. This lack of specificity is consistent with the fact that early folding transitions of the *Tetrahymena* ribozyme are not affected by mutations that destroy key tertiary interactions in the RNA.[8,38]

The second transition to the native state of the *Tetrahymena* ribozyme is not only more cooperative than the first transition, but very sensitive to the size and valence of the counterion. This result agrees with previous studies on the *Tetrahymena* ribozyme using native gel electrophoresis, in which the stability of the folded RNA increased with the counterion charge density.[18,20] Although the folding equilibria measured by SAXS change less steeply with ion concentration (smaller n) because of the higher RNA concentration used for SAXS studies, the trends among the ions are the same in both types of experiments. The sensitivity of the *Tetrahymena* ribozyme to counterion size may be augmented by structural motifs, such as P5abc, that are specifically stabilized by Mg^{2+}.[24,58,59]

Since specific collapse transitions produce compact, well-folded structures, they are expected to depend more strongly on the excluded volume of

the counterions and the strength of their interaction with the electrostatic field of the RNA.[22] By contrast, nonspecific collapse depends on the valence of the counterions, as expected from polyelectrolyte effects, but is insensitive to their size. The importance of counterion charge density in RNA folding transitions can be observed in other RNAs. For example, the catalytic domain of the *Bacillus subtilis* RNase P ribozyme, which also folds through I's that are nearly as compact as N, is more stable in Mg^{2+} and Ca^{2+} than in Sr^{2+} and Ba^{2+}.[47]

The collapse transition in the *Azoarcus* ribozyme also depends on counterion size and valence, consistent with a native-like I_C. However, it is less sensitive to differences among multivalent ions than the *Tetrahymena* ribozyme. This difference in the two RNAs may be due to the greater stability of the *Azoarcus* folding intermediates, which allow the core helices to assemble correctly before tertiary folding is complete. Consequently, the *Azoarcus* ribozyme achieves its native topology earlier in the folding process than the *Tetrahymena* ribozyme.

While the SAXS data reported here agree well with biochemical and spectroscopic studies of the folding transitions, two interesting discrepancies in the results obtained by these methods raise questions for future studies. First, we find that R_g and $P(r)$ for the folded state are similar in all of the counterions tested, yet the electrophoretic mobility of the folded RNA is much greater in Mg^{2+} than in Sr^{2+}.[22] The folded RNA may be more flexible in counterions with low charge density.[60] It will be interesting to know how counterions influence the RNA dynamics. Both the *Tetrahymena* and RNase P ribozymes refold more rapidly in Ba^{2+} than in Mg^{2+}.[47,61] Second, Ca^{2+} drives collapse of both ribozymes as effectively as Mg^{2+} in the SAXS experiments. However, Mg^{2+} is more effective than Ca^{2+} when folding is probed biochemically.[22,36] A similar difference is observed for Sr^{2+} and Ba^{2+}. Counterion hydration may influence the compactness of the polynucleotide chain in solution.

In conclusion, these and other studies show that polyelectrolyte effects provide a strong driving force for RNA compaction, but sequence-specific interactions within the RNA determine whether it forms a specific, compact structure. For group I ribozymes (and likely many other RNAs), the native fold is more compact than nonnative folds. Because structures that are more compact are more sensitive to the counterion valence and size, the counterion effects are amplified when the RNA can fold specifically. This suggests how ion mixtures and even neutral osmolytes may fine-tune the balance between competing structures in RNA.

Materials and Methods

Sample preparation and SAXS experiments

The *Azoarcus* ribozyme (195 nt) and *Tetrahymena* L-21 Sca ribozyme (389 nt) were prepared by T7 transcription as previously described.[34,62] After gel purification, the RNA was concentrated and exchanged multiple times with 20 mM Tris–HCl (pH 7.5). SAXS measurements [0.4 mg/ml RNA in 20 mM Tris–HCl (pH 7.5)] were carried out at the Advanced Photon Source at ID18 (BioCAT) as previously described.[9] The *Azoarcus* ribozyme was equilibrated for 5 min at 32 °C with each addition of titrant before acquisition of data. The *Tetrahymena* ribozyme was equilibrated for 15 min at 50 °C, then cooled to room temperature (>5 min) before the acquisition of data at 32 °C.

Data analysis

Raw data were corrected for detector sensitivity and geometrical factors and circularly averaged. Following the subtraction of background scattering from the buffer, scattering curves were inverted using GNOM[63]† to obtain the normalized distance distribution function $P(r)$:

$$P(r) = \frac{1}{2\pi^2}\int_{Q_{\min}}^{Q_{\max}} I(Q)Qr\sin(Qr)\mathrm{d}Q \qquad (1)$$

in which the scattering vector is $Q=(4\pi/\lambda)\sin(\theta)$, λ is the wavelength and 2θ is the scattering angle. $P(r)$ is assumed to differ from zero only in the interval $D_{\min}<r<D_{\max}$. For a given $D_{\min}$ and $D_{\max}$ the calculated $I(Q)$ is:

$$I_{\mathrm{calc}}(Q) = \int_{D_{\min}}^{D_{\max}} \frac{1}{r^2}P(r)e^{-iQr}\mathrm{d}r \qquad (2)$$

We determined $D_{\max}$ by iteratively optimizing the goodness of the fit between the experimental scattering data and the calculated scattering values, I_{calc}. The optimum value for $D_{\max}$ is sensitive to the Q range, which in this study was 0.008–0.11 $Å^{-1}$. Over this range the data are smooth.

The square of the radius of gyration, R_g, was calculated from the second moment of $P(r)$ using:

$$R_g^2 = \frac{\int_{D_{\min}}^{D_{\max}} P(r)r^2\mathrm{d}r}{2\int_{D_{\min}}^{D_{\max}} P(r)\mathrm{d}r} \qquad (3)$$

The R_g values from Eq. (3) agreed well with those calculated by the Guinier approximation, validating the choice of $D_{\max}$.

Folding equilibria

For the *Azoarcus* ribozyme, the fractions unfolded (ϕ_U) and folded (ϕ_N) RNA at each ion concentration were calculated from $R_g^2=\phi_U R_{g,U}^2+\phi_F R_{g,N}^2$, in which $R_{g,U}$ and $R_{g,N}$ are the radii of gyration for the unfolded and folded RNA.[7] $R_g(U)$ was assumed to vary with ion concentration, $R_g(U)=\alpha-\beta\log C$, in which α and β are constants obtained from the data at low C (see Fig. S2). The midpoints and cooperativity of the folding equilibria

† http://www.embl-hamburg.de/ExternalInfo/Research/Sax/

with respect to ion concentration[45] were obtained by fitting ϕ_N to the Hill equation:

$$\phi_N = \phi_N(0) + [\phi_N(\max) - \phi_N(0)]\left[\frac{(C/C_m)^n}{1+(C/C_m)^n}\right] \quad (4)$$

in which C_m is the midpoint, n is the Hill constant, and $\phi_N(0)$ and $\phi_N(\max)$ are the minimum and maximum values of the function, respectively.

For the *Tetrahymena* ribozyme, the data were fit to a three-state model (U⇔I⇔N) in which $R_g^2 = \phi_U R_{g,U}^2 + \phi_I R_{g,I}^2 + \phi_F R_{g,N}^2$, and ϕ_U, ϕ_I, and ϕ_N are the fractions of unfolded, intermediate, and folded *Tetrahymena* ribozyme at each ion concentration. The ion-dependence of folding is described by the partition function

$$Z = 1 + (C/C_1)^{n_1} + (C/C_2)^{n_2} \quad (5)$$

in which C is the counterion concentration, C_i are reference concentrations and n_i are cooperativity parameters that define the statistical weights of the I and N species relative to the U state.[44] These parameters and $R_{g,I}$ were evaluated by fitting the experimental R_g^2 *versus* counterion concentration to:

$$R_g^2 = \frac{R_{g,U}^2 + R_{g,I}^2(C/C_1)^{n_1} + R_{g,N}^2(C/C_2)^{n_2}}{1+(C/C_1)^{n_1}+(C/C_2)^{n_2}} \quad (6)$$

(see Table SII). The midpoints of the U to I and I to N transitions (Table 2) were obtained by calculating ϕ_U, ϕ_I, and ϕ_N from the parameters of the three-state model and fitting ϕ_U *versus* C and ϕ_N *versus* C to Eq. (4).

Singular value decomposition

We used SVD to assess the minimum number of components needed to describe the scattering data, as previously described for SAXS data on proteins.[64] Each column of matrix $A(Q,k)$ represents the scattering intensity, $I(Q)$, measured as a function of Q at counterion concentration k. We verified that the order of scattering intensities in the matrix $A(Q,k)$ was irrelevant for the final results. The data were represented as $A = USV^T$, in which S is a diagonal matrix of singular values. $U(Q,k)$ forms a complete set of basis functions in which the scattering spectra can be constructed as a linear superposition of the basis functions at each k. Each column of the product of SV^T determines the Mg^{2+} concentration-dependent coefficients corresponding to each basis function. The scattering profile at each counterion concentration, k, can be approximated as:

$$I_{calc}(Q,k) = \sum_{j=1}^{L} U_j s_j V_{kj} \quad (7)$$

where L is the minimum number of components needed to represent the scattering spectra, U_j is the jth basis function, and the dependence of U_j on concentration k is depicted by $s_j V_{kj}$. The minimum number of basis functions that effectively represent the data was determined based on the shape of the basis functions, the number of significant singular values, the autocorrelations of U, and the value of chi-squared, χ^2, which is the deviation between the experimental and SVD constructed scattering data. Chi-squared was computed from:

$$\chi^2 = \frac{1}{m\times(n-L)}\sum_{k=1}^{m}\sum_{i=1}^{m}\left(\frac{I_{exp}^k(Q_i) - I_{calc,n}^k(Q_i)}{\sigma_i}\right)^2 \quad (8)$$

in which σ_i is the error associated with the scattering intensity at each momentum transfer, Q. The autocorrelation of U was calculated as:

$$C(U_i) = \sum_{j=1}^{m-1} U_{j,i}U_{j+1,i} \quad (9)$$

In assessing the goodness of the fits, both the autocorrelation of U and χ^2 values should be close to unity, although the exact value is not critical.[64,65]

Persistence length

The persistence lengths l_p were extracted from the distance distribution functions $P(r)$ obtained from the SAXS data, as previously described.[5] The $P(r)$ curves at each ion concentration were fit to the theoretical expression for the end-to-end distance distribution of a worm-like chain (WLC), for large $x = l_p r/R_g^2$, in which:

$$P(x) \sim \exp\left(-1/\left(1-x^2\right)\right) \quad (10)$$

Acknowledgements

The authors thank E. Kondrashkina and T. Irving (BioCAT), S. Seifert (BESSRC) and U. Perez-Salas for assistance with SAXS experiments, and R. Behrouzi for help with data analysis. This work was supported by DOC (R.M.B), NSF (D.T.) and NIGMS (S.A.W.). BioCAT is supported by the NIH (RR-08630). Use of the Advanced Photon Source was supported by the U.S. DOE under contract No. W-31-109-ENG-38.

Supplementary Data

Supplementary data associated with this article can be found, in the online version, at doi:10.1016/j.jmb.2009.08.044

References

1. Thirumalai, D. & Hyeon, C. (2005). RNA and protein folding: common themes and variations. *Biochemistry*, **44**, 4957–4970.
2. Li, P. T., Vieregg, J. & Tinoco, I., Jr (2008). How RNA unfolds and refolds. *Annu. Rev. Biochem.* **77**, 77–100.
3. Sosnick, T. R. (2008). Kinetic barriers and the role of topology in protein and RNA folding. *Protein Sci.* **17**, 1308–1318.
4. Draper, D. E., Grilley, D. & Soto, A. M. (2005). Ions and RNA folding. *Annu. Rev. Biophys. Biomol. Struct.* **34**, 221–243.
5. Caliskan, G., Hyeon, C., Perez-Salas, U., Briber, R. M., Woodson, S. A. & Thirumalai, D. (2005). Persistence length changes dramatically as RNA folds. *Phys. Rev. Lett.* **95**, 268303.
6. Buchmueller, K. L., Webb, A. E., Richardson, D. A. & Weeks, K. M. (2000). A collapsed, non-native RNA folding state. *Nat. Struct. Biol.* **7**, 362–366.

7. Fang, X., Littrell, K., Yang, X. J., Henderson, S. J., Siefert, S., Thiyagarajan, P. *et al.* (2000). Mg^{2+}-dependent compaction and folding of yeast $tRNA^{Phe}$ and the catalytic domain of the *B. subtilis* RNase P RNA determined by small-angle X-ray scattering. *Biochemistry*, **39**, 11107–11113.
8. Das, R., Kwok, L. W., Millett, I. S., Bai, Y., Mills, T. T., Jacob, J. *et al.* (2003). The fastest global events in RNA folding: electrostatic relaxation and tertiary collapse of the *Tetrahymena* ribozyme. *J. Mol. Biol.* **332**, 311–319.
9. Chauhan, S., Caliskan, G., Briber, R. M., Perez-Salas, U., Rangan, P., Thirumalai, D. & Woodson, S. A. (2005). RNA tertiary interactions mediate native collapse of a bacterial group I ribozyme. *J. Mol. Biol.* **353**, 1199–1209.
10. Kwok, L. W., Shcherbakova, I., Lamb, J. S., Park, H. Y., Andresen, K., Smith, H. *et al.* (2006). Concordant exploration of the kinetics of RNA folding from global and local perspectives. *J. Mol. Biol.* **355**, 282–293.
11. Thirumalai, D., Lee, N., Woodson, S. A. & Klimov, D. (2001). Early events in RNA folding. *Annu. Rev. Phys. Chem.* **52**, 751–762.
12. Woodson, S. A. (2005). Metal ions and RNA folding: a highly charged topic with a dynamic future. *Curr. Opin. Chem. Biol.* **9**, 104–109.
13. Chen, S. J. (2008). RNA folding: conformational statistics, folding kinetics, and ion electrostatics. *Annu. Rev. Biophys.* **37**, 197–214.
14. Chu, V. B. & Herschlag, D. (2008). Unwinding RNA's secrets: advances in the biology, physics, and modeling of complex RNAs. *Curr. Opin. Struct. Biol.* **18**, 305–314.
15. Anderson, C. F. & Record, M. T. (1995). Salt nucleic-acid interactions. *Annu. Rev. Phys. Chem.* **46**, 657–700.
16. Bloomfield, V. A. (1997). DNA condensation by multivalent cations. *Biopolymers*, **44**, 269–282.
17. Manning, G. S. (2003). Comments on selected aspects of nucleic acid electrostatics. *Biopolymers*, **69**, 137–143.
18. Heilman-Miller, S. L., Thirumalai, D. & Woodson, S. A. (2001). Role of counterion condensation in folding of the *Tetrahymena* ribozyme. I. Equilibrium stabilization by cations. *J. Mol. Biol.* **306**, 1157–1166.
19. Rouzina, I. & Bloomfield, V. A. (1996). Influence of ligand spatial organization on competitive electrostatic binding to DNA. *J. Phys. Chem.* **100**, 4305–4313.
20. Koculi, E., Lee, N. K., Thirumalai, D. & Woodson, S. A. (2004). Folding of the *Tetrahymena* ribozyme by polyamines: importance of counterion valence and size. *J. Mol. Biol.* **341**, 27–36.
21. Tan, Z. J. & Chen, S. J. (2006). Ion-mediated nucleic acid helix-helix interactions. *Biophys. J.* **91**, 518–536.
22. Koculi, E., Hyeon, C., Thirumalai, D. & Woodson, S. A. (2007). Charge density of divalent metal cations determines RNA stability. *J. Am. Chem. Soc.* **129**, 2676–2682.
23. Manning, G. S. (1978). The molecular theory of polyelectrolyte solutions with applications to the electrostatic properties of polynucleotides. *Q. Rev. Biophys.* **11**, 179–246.
24. Cate, J. H., Hanna, R. L. & Doudna, J. A. (1997). A magnesium ion core at the heart of a ribozyme domain. *Nat. Struct. Biol.* **4**, 553–558.
25. Bukhman, Y. V. & Draper, D. E. (1997). Affinities and selectivities of divalent cation binding sites within an RNA tertiary structure. *J. Mol. Biol.* **273**, 1020–1031.
26. Shiman, R. & Draper, D. E. (2000). Stabilization of RNA tertiary structure by monovalent cations. *J. Mol. Biol.* **302**, 79–91.
27. Serra, M. J., Baird, J. D., Dale, T., Fey, B. L., Retatagos, K. & Westhof, E. (2002). Effects of magnesium ions on the stabilization of RNA oligomers of defined structures. *RNA*, **8**, 307–323.
28. Stahley, M. R., Adams, P. L., Wang, J. & Strobel, S. A. (2007). Structural metals in the group I intron: a ribozyme with a multiple metal ion core. *J. Mol. Biol.* **372**, 89–102.
29. Celander, D. W. & Cech, T. R. (1991). Visualizing the higher order folding of a catalytic RNA molecule. *Science*, **251**, 401–407.
30. Zarrinkar, P. P. & Williamson, J. R. (1994). Kinetic intermediates in RNA folding. *Science*, **265**, 918–924.
31. Pan, J. & Woodson, S. A. (1998). Folding intermediates of a self-splicing RNA: mispairing of the catalytic core. *J. Mol. Biol.* **280**, 597–609.
32. Russell, R., Millett, I. S., Tate, M. W., Kwok, L. W., Nakatani, B., Gruner, S. M. *et al.* (2002). Rapid compaction during RNA folding. *Proc. Natl Acad. Sci. USA*, **99**, 4266–4271.
33. Rangan, P., Masquida, B., Westhof, E. & Woodson, S. A. (2003). Assembly of core helices and rapid tertiary folding of a small bacterial group I ribozyme. *Proc. Natl Acad. Sci. USA*, **100**, 1574–1579.
34. Perez-Salas, U. A., Rangan, P., Krueger, S., Briber, R. M., Thirumalai, D. & Woodson, S. A. (2004). Compaction of a bacterial group I ribozyme coincides with the assembly of core helices. *Biochemistry*, **43**, 1746–1753.
35. Rook, M. S., Treiber, D. K. & Williamson, J. R. (1999). An optimal Mg^{2+} concentration for kinetic folding of the *Tetrahymena* ribozyme. *Proc. Natl Acad. Sci. USA*, **96**, 12471–12476.
36. Rangan, P. & Woodson, S. A. (2003). Structural requirement for Mg^{2+} binding in the group I intron core. *J. Mol. Biol.* **329**, 229–238.
37. Shcherbakova, I., Gupta, S., Chance, M. R. & Brenowitz, M. (2004). Monovalent ion-mediated folding of the *Tetrahymena thermophila* ribozyme. *J. Mol. Biol.* **342**, 1431–1442.
38. Takamoto, K., Das, R., He, Q., Doniach, S., Brenowitz, M., Herschlag, D. & Chance, M. R. (2004). Principles of RNA compaction: insights from the equilibrium folding pathway of the p4–p6 RNA domain in monovalent cations. *J. Mol. Biol.* **343**, 1195–1206.
39. Putnam, C. D., Hammel, M., Hura, G. L. & Tainer, J. A. (2007). X-ray solution scattering (SAXS) combined with crystallography and computation: defining accurate macromolecular structures, conformations and assemblies in solution. *Q. Rev. Biophys.* **40**, 191–285.
40. Lipfert, J. & Doniach, S. (2007). Small-angle X-ray scattering from RNA, proteins, and protein complexes. *Annu. Rev. Biophys. Biomol. Struct.* **36**, 307–327.
41. Wilhelm, P., Pilz, I., Degovics, G. & von der Haar, F. (1982). Small- and large-angle X-ray scattering studies of counter ion influence on tRNA conformation. *Z. Naturforsch., C: Biosci.* **37**, 1293–1296.
42. Russell, R., Millett, I. S., Doniach, S. & Herschlag, D. (2000). Small angle X-ray scattering reveals a compact intermediate in RNA folding. *Nat. Struct. Biol.* **7**, 367–370.
43. Adams, P. L., Stahley, M. R., Kosek, A. B., Wang, J. & Strobel, S. A. (2004). Crystal structure of a self-splicing group I intron with both exons. *Nature*, **430**, 45–50.
44. Chauhan, S., Behrouzi, R., Rangan, P. & Woodson, S. A. (2009). Structural rearrangements linked to global folding pathways of the Azoarcus group I ribozyme. *J. Mol. Biol.* **386**, 1167–1178.

45. Pan, J., Thirumalai, D. & Woodson, S. A. (1999). Magnesium-dependent folding of self-splicing RNA: exploring the link between cooperativity, thermodynamics, and kinetics. *Proc. Natl Acad. Sci. USA*, **96**, 6149–6154.
46. Brion, P. W. E. (1997). Hierarchy and dynamics of RNA folding. *Annu. Rev. Biophys. Biomol. Struct.* **26**, 113.
47. Fang, X. W., Thiyagarajan, P., Sosnick, T. R. & Pan, T. (2002). The rate-limiting step in the folding of a large ribozyme without kinetic traps. *Proc. Natl Acad. Sci. USA*, **99**, 8518–8523.
48. Lehnert, V., Jaeger, L., Michel, F. & Westhof, E. (1996). New loop-loop tertiary interactions in self-splicing introns of subgroup IC and ID: a complete 3D model of the *Tetrahymena thermophila* ribozyme. *Chem. Biol.* **3**, 993–1009.
49. Svergun, D. I., Barberato, C. & Koch, M. H. J. (1995). CRYSOL—a program to evaluate X-ray solution scattering of biological macromolecules from atomic coordinates. *J. Appl. Crystallogr.* **28**, 768–773.
50. Liphardt, J., Onoa, B., Smith, S. B., Tinoco, I. J. & Bustamante, C. (2001). Reversible unfolding of single RNA molecules by mechanical force. *Science*, **292**, 733–737.
51. Hyeon, C., Dima, R. I. & Thirumalai, D. (2006). Size, shape, and flexibility of RNA structures. *J. Chem. Phys.* **125**, 194905.
52. Treiber, D. K. & Williamson, J. R. (1999). Exposing the kinetic traps in RNA folding. *Curr. Opin. Struct. Biol.* **9**, 339–345.
53. Woodson, S. A. & Rangan, P. (2008). Folding mechanisms of group I ribozymes. In (Lilley, D. M. J. & Eckstein, F., eds), pp. 295–314, RSC Publishing, Cambridge, UK.
54. Woodson, S. A. (2000). Recent insights on RNA folding mechanisms from catalytic RNA. *Cell Mol. Life Sci.* **57**, 796–808.
55. Sclavi, B., Sullivan, M., Chance, M. R., Brenowitz, M. & Woodson, S. A. (1998). RNA folding at millisecond intervals by synchrotron hydroxyl radical footprinting. *Science*, **279**, 1940–1943.
56. Downs, W. D. & Cech, T. R. (1996). Kinetic pathway for folding of the *Tetrahymena* ribozyme revealed by three UV-inducible crosslinks. *RNA*, **2**, 718–732.
57. Rook, M. S., Treiber, D. K. & Williamson, J. R. (1998). Fast folding mutants of the *Tetrahymena* group I ribozyme reveal a rugged folding energy landscape. *J. Mol. Biol.* **281**, 609–620.
58. Johnson, T. H., Tijerina, P., Chadee, A. B., Herschlag, D. & Russell, R. (2005). Structural specificity conferred by a group I RNA peripheral element. *Proc. Natl Acad. Sci. USA*, **102**, 10176–10181.
59. Uchida, T., He, Q., Ralston, C. Y., Brenowitz, M. & Chance, M. R. (2002). Linkage of monovalent and divalent ion binding in the folding of the P4–P6 domain of the *Tetrahymena* ribozyme. *Biochemistry*, **41**, 5799–5806.
60. Koculi, E., Thirumalai, D. & Woodson, S. A. (2006). Counterion charge density determines the position and plasticity of RNA folding transition states. *J. Mol. Biol.* **359**, 446–454.
61. Heilman-Miller, S. L., Pan, J., Thirumalai, D. & Woodson, S. A. (2001). Counterion condensation in folding of the *Tetrahymena* ribozyme. II. Counterion dependence of folding kinetics. *J. Mol. Biol.* **309**, 57–68.
62. Zaug, A. J., Grosshans, C. A. & Cech, T. R. (1988). Sequence-specific endoribonuclease activity of the *Tetrahymena* ribozyme: enhanced cleavage of certain oligonucleotide substrates that form mismatched ribozyme-substrate complexes. *Biochemistry*, **27**, 8924–8931.
63. Semenyuk, A. V. & Svergun, D. I. (1991). GNOM—a program package for small-angle scattering data-processing. *J. Appl. Crystallogr.* **24**, 537–540.
64. Segel, D. J., Eliezer, D., Uversky, V., Fink, A. L., Hodgson, K. O. & Doniach, S. (1999). Transient dimer in the refolding kinetics of cytochrome *c* characterized by small-angle X-ray scattering. *Biochemistry*, **38**, 15352–15359.
65. Paliwal, A., Asthagiri, D., Bossev, D. P. & Paulaitis, M. E. (2004). Pressure denaturation of staphylococcal nuclease studied by neutron small-angle scattering and molecular simulation. *Biophys. J.* **87**, 3479–3492.